Visible-light induced photochemistry of Electron Donor-Acceptor Complexes in Perfluoroalkylation Reactions: Investigation of halogen bonding interactions through UV–Visible absorption and Raman spectroscopies combined with DFT calculations

Thierry Tassaing, Joseph Grondin, Christian Aupetit, Jean-Marc Vincent, Raphael Méreau

Visible-light induced photochemistry of Electron Donor-Acceptor Complexes in Perfluoroalkylation Reactions: Investigation of halogen bonding interactions through UV-Visible absorption and Raman spectroscopies combined with DFT calculations

Joseph Grondin, Christian Aupetit, Jean-Marc Vincent, Raphael Méreau, Thierry Tassaing*

Institut des Sciences Moléculaires, UMR CNRS 5255, Université de Bordeaux, 351 cours de la Libération 33405 Talence Cedex, France

** Corresponding author: thierry.tassaing@u-bordeaux.fr*

ABSTRACT

Visible light promoted perfluoroalkylation reactions initiated via halogen bonding interactions between perfluoroalkyl iodides (Rf–I, Rf=C_nF_{2n+1}) and Lewis bases have been recognized as a powerful tool in the field of radical synthetic chemistry. In order to provide some insights into the nature, strength and role in the activation process of halogen bonding interactions, we have performed a combined UV-Visible/Raman/DFT study on a model Rf–I (C_4F_9I) and a series of Lewis bases (LB) frequently used for the activation of perfluoroalkylation reactions, including DBU, MTBD, TMG, TMEDA and Et_3N. Raman studies conducted in acetonitrile solutions show that the band at 279 cm^{-1} associated with the C−I stretching normal mode of C_4F_9I shifts about 20 cm^{-1} towards lower wavenumbers upon formation of the halogen-bonded complexes. Additionally, the Raman study revealed that at concentrations typically used for perfluoroalkylation reactions, the [C_4F_9I-LB] complexes are the main species present in solution. UV-Vis spectroscopy revealed that complex formation is characterized by a strong increase in absorption from 225 - 350 nm. The higher the basicity of the Lewis base, the higher the increase of the UV absorbance.

Keywords: EDA complexes, Halogen bonding, UV-Visible, Raman spectroscopy, DFT calculations, Perfluoroalkylation

1. INTRODUCTION

During the last decade, many photochemical methods involving photocatalysts that harvest visible light energy to activate substrates and generate reactive radicals [1] have been developed.[2-5] More recently, photochemical processes using electron donor−acceptor (EDA) complexes have been recognized as a powerful tool in the field of visible light-driven radical synthetic chemistry. The potential of EDA complex photochemistry has been recently critically assessed by Melchiorre et al [6]. Electron donor−acceptor (EDA) complexes, also called “Charge Transfer complexes” as initially proposed by Mulliken,[7] result from an

interaction between an electron acceptor A (Lewis acid) and a donor molecule D (Lewis base). EDA complexes are characterized by the appearance of an absorption band that is red-shifted compared to the absorption bands of the individual A and D components. Thus, light excitation in the EDA complex electronic absorption band can trigger an intramolecular single-electron-transfer (SET) to generate radical species under mild conditions, typically visible light irradiation. A recent review by Postigo [8] focuses on EDA complexes that result from halogen-bonding interactions[9] between Lewis organic bases and perfluoroalkyl iodides (Rf–I). Upon visible light-excitation a SET takes place to generate Rf radicals involved in ATRA (Atom Transfer Radical Addition) and ATRE (Atom Transfer Radical Elimination) reactions. Exploiting EDA complexes in light-mediated processes thus emerges as an activation concept which could simplify reaction conditions by avoiding the use of organic or organometallic photocatalysts. However, as highlighted by Postigo, a clear understanding of the visible light induced photochemistry using the halogen bonded EDA complex concept is still lacking. Indeed, in many examples, even identification of the species responsible for the absorption of visible light remains unclear. In most cases, the radical initiating chain is attributed to a species with a very low extinction coefficient at the irradiation source (visible light). In addition, in many studies using compact fluorescent light (CFL) bulbs as the light source, it is not clear whether the irradiation wavelength responsible for the generation of the active radical species is in the UVA or the visible range, as this type of low-pressure mercury lamp emits both visible and UVA photons. In this context, the case of radical perfluoroalkylation reactions is of particular interest. While numerous visible light-promoted perfluoroalkylations involve halogen bonding interactions between Rf–I and a variety of Lewis bases having lone pairs of electrons centered on oxygen,[10, 11] nitrogen,[12-16] or phosphorus[17, 18]) atoms, a detailed understanding of the mechanism at work in these photochemical processes is still required.

Characterization of the postulated EDA complexes is typically conducted using UV-Visible spectroscopy in order to identify a possible bathochromic shift and/or the appearance of a new electronic absorption band.[10, 17, 19] ^{19}F NMR spectroscopy was also employed, as the weakening of the I–CF_2 bond resulting from the halogen bonding leads to an upfield shift of the CF_2 group resonance. Binding constants and stoichiometries of RfI-Lewis base complexes were conveniently assessed by ^{19}F NMR titration and Job's plots, respectively.[12],[[20]

Raman spectroscopy is much less exploited to characterize EDA complexes, and can allow direct monitoring of the low frequency C–I stretching normal mode of iodoperfluoroalkanes detected at about 250 cm^{-1} [21] that is red-shifted upon halogen bonding interactions.[22]

Finally, DFT calculations can be performed in order to evidence the formation of EDA complexes, and in particular evaluate interaction energies, as well as to simulate IR, Raman and UV-Visible spectra.[18, 23, 24]

All these considerations prompted us to perform a combined UV-Visible, Raman and DFT study in order to gain some insights into the halogen bond interaction between a model Rf−I, namely C_4F_9I, and a series of strong Lewis bases, including:- tertiary amines - triethylamine (Et_3N) and N,N,N',N'-tetramethylethylendiamine (TMEDA), amidine 1,8-diazabicyclo(5.4.0)undec-7-ene (DBU), and guanidines 1,1,3,3-tetramethylguanidine (TMG) and 7-Methyl-1,5,7triazabicyclo(4.4.0)dec-5-ene (MTBD). For comparison, we also performed DFT calculations on a series of weaker Lewis bases such as aniline, pyridine, propylene oxide, tetrahydrofuran (THF), acetone and dimethylacetamide (DMA). The latter two being used recently for the activation of perfluoroalkylation reactions.[10, 11] By combining this set of experimental and theoretical approaches, we determined the strength of the halogen bond interactions occurring between C_4F_9I and Lewis bases, and revealed how it affects the UV-Visible spectrum of the Rf–I for its possible activation by visible light to generate Rf radicals.

2. EXPERIMENTAL AND CALCULATION SECTION

2.1. Materials

Acetonitrile (CH_3CN, Sigma Aldrich), 1,8-diazabicyclo[5.4.0]undec-7-ene (DBU, Alfa Aesar), triethylamine (Et_3N, Sigma Aldrich), 7-methyl-1,5,7-triazabicyclo[4.4.0]dec-5-ene (MTBD, Sigma Aldrich), tetramethylguanidine (TMG, Alfa Aesar), tetramethylethylenediamine, (TMEDA, Sigma Aldrich), were used without further purification.

2.2. Spectroscopic methods

UV-Vis spectra were measured in the spectral range from 225 - 1000 nm using an Ocean Optics QE64000 UV-VIS spectrometer in Hellma cuvettes (10 x 10 mm, Suprasil quartz glass) or in a home-made transmission liquid cell built with sapphire windows with a pathlength of 75 μm.

The Raman experiments were recorded using a Jobin-Yvon Horiba XploRA confocal Raman microscope equipped with a 10X objective and a laser diode at a wavelength λ = 785 nm and 100 % laser power of 45 mW. The spectral range from 140 to 1280 cm^{-1} was recorded with a grating of 1200 l/mm and a resolution of about 3 cm^{-1}. The spectra result from two acquisitions of 20 seconds each to improve the signal-to-noise ratio.

2.3. Computational details

Preliminary calculations of equilibrium structures were performed using a semi-empirical model (AM1) to determine the most stable conformations. The lowest energy structures obtained at the AM1 level using the AMPAC software were further investigated using the Density Functional Theory method (DFT) implemented in the Gaussian 09 package. DFT calculations of geometries, energies, and vibrational frequencies reported in this paper were carried out with the M06-2X functional using the DGDZVP basis set. All frequencies of each structure have also been calculated to verify the absence of imaginary frequency for ground states structures. Stabilization energies of the C_4F_9I-Lewis base complexes investigated in this paper were calculated using the "supermolecule" method as the difference in energy between each complex and the sum of the isolated monomers.

3. RESULTS AND DISCUSSION

3.1. UV-Visible measurements

Figure 1 shows the evolution of the absorption spectra of a solution of C_4F_9I in CH_3CN upon addition of increasing amounts of Et_3N or DBU. The spectrum of Et_3N displays a weak absorption tail in the range 225-250 nm (figure 1A) that is associated to the $n \rightarrow \sigma^*$ electronic

transition involving the lone pair and the C−N bond, whose maximum was identified by Tannebaum et al. [25] to be at about 210 nm. The absorption maximum of the n→σ* electronic transition involving a lone pair and the C−I bond of C_4F_9I is observed at about 265 nm.[17] Upon addition of increasing quantities of Et_3N, an increased intensity of the UV absorption is observed. The band at 265 nm is blue-shifted to 250 nm concomitantly with the appearance of a band at about 290 nm. Overall, the presence of Et_3N leads to a significant increase of light absorption in the range 225 - 350 nm.

The spectrum of DBU displays a band centered at 240 nm that is associated to the n→π* electronic transition involving the C=N bond (figure 1B).[26] Upon addition of increasing amounts of DBU to the C_4F_9I-CH_3CN mixture, a strong increase of the intensity and broadening of the UV absorption is observed. At the lowest DBU concentration, the absorption is enhanced and blue-shifted to 250 nm. A further increase of the DBU concentration leads to an additional increase of the absorption that is red-shifted to 270 nm at the highest concentration. Simultaneously, an additional band appears at about 290 nm that increases with the concentration of DBU. Overall, the presence of DBU leads to a significant increase of light absorption in the 225-350 nm region.

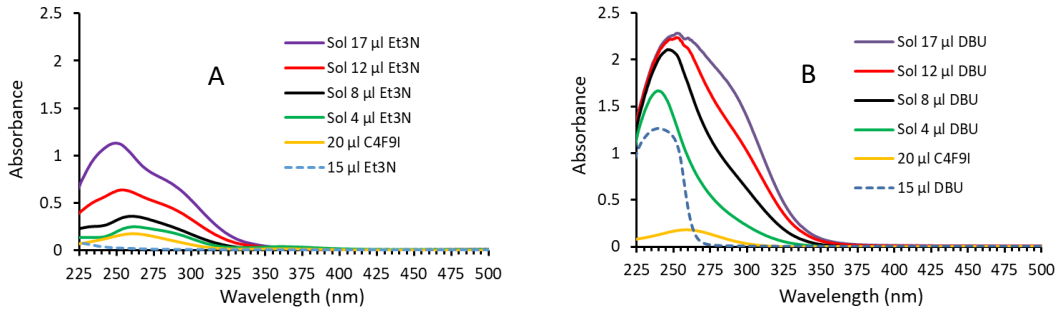

Figure 1: UV-Vis absorption spectra of solutions of C_4F_9I (20 µl) in CH_3CN (1 ml) containing increasing amounts of Et_3N (A) or DBU (B) (Transmission cell, pathlength 75 µm).

Comparison of the spectra in the presence of other Lewis bases is reported in figure 2. The use of TMG, TMEDA and MTBD leads to a similar increase of absorbance to that of DBU, although for TMG the appearance of the band at ~ 290 nm is less pronounced. Thus, when considering the UV spectra, the absorbance is red-shifted and strongly enhanced in the presence of the Lewis bases. For comparison, the absorbance at 325 nm of the C_4F_9I solutions are in the order : "free" C_4F_9I (A ~ 0.001) < C_4F_9I-Et_3N (A = 0.16) ~ C_4F_9I-TMEDA (A = 0.17) < C_4F_9I-TMG (A = 0.25) < C_4F_9I-DBU (A = 0.45) < C_4F_9I-MTBD (A = 0.55). Considering that TMEDA has two equivalent tertiary amine groups, the absorbance observed for the C_4F_9I-TMEDA has been divided by two for a better comparison of the absorbance at 325 nm of all complexes. Interestingly, the change in absorbance at 325 nm is correlated with the pKa of the LB, i.e. pKa (Et_3N) = 18.8 ~ pKa (TMEDA) = 18.7 < pKa (TMG) = 23.3 < pKa (DBU) = 24.3 < pKa (MTBD) = 25.5. In other words, the higher the basicity of the Lewis base, the higher the increase of the UV absorbance.

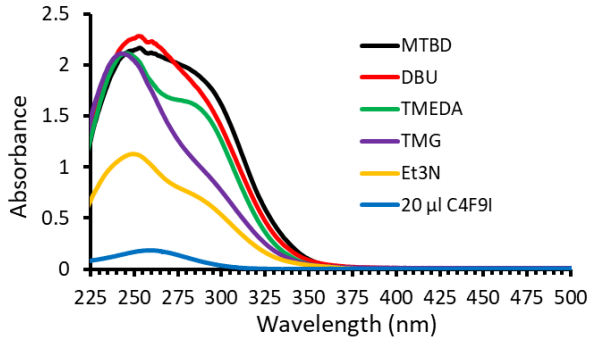

Figure 2: UV-Vis absorption spectra of solutions of C_4F_9I (20 µl) in CH_3CN (1 ml) containing Lewis bases (0.1 M). (Transmission cell, pathlength 75 µm). The spectrum of C_4F_9I is reported for comparison.

In order to be more sensitive to absorption changes above 350 nm, we carried out UV−vis measurements on more concentrated solutions and using a quartz cuvette with a path length of 10 mm (figure 3). Notably, such conditions are more representative of the experimental conditions used for perfluoroalkylation reactions. Interestingly, while for both bases an increased absorption is observed between 350 - 400 nm upon increasing their concentration, with DBU the solution turned from colourless to yellow due to the appearance a broad band (λ_{max} ~ 420 nm) in the blue region of the visible spectrum (see figure 3 for a comparison between NEt_3 and DBU). At high concentration, the intensity of the broad electronic absorption centered at 420 nm increases smoothly during 10 h (see ESI 1), indicating that new species are formed by reaction between DBU and C_4F_9I. Previous works suggest that *N*-perfluoroalkylation of DBU occurs to deliver the *N*-perfluoroalkylated iminium **1** and/or its enamine derivative **2** (see ESI 2).[27, 28] The yellow color which develops over time might be ascribed to the formation of a EDA complex between the enamine and unreacted C_4F_9I.[6] Further work, beyond the scope of this study, will be required to ascertain this particular issue.

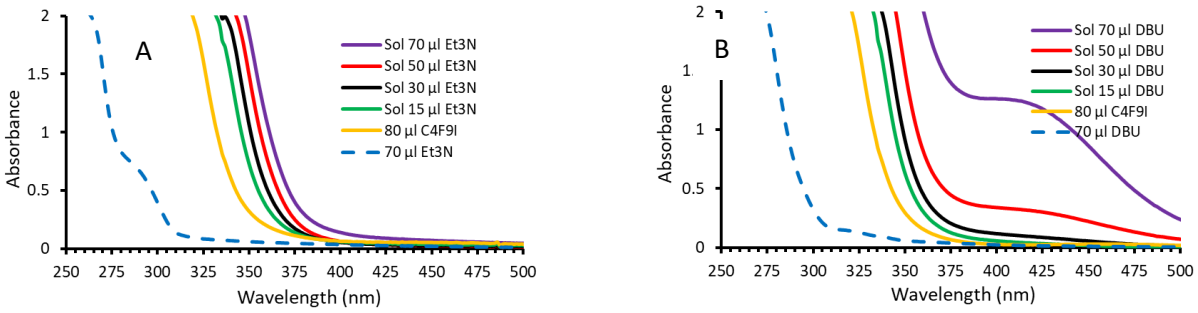

Figure 3: UV-Vis absorption spectra of solutions of C_4F_9I (80 µl, 0.46 M) in CH_3CN (1 ml) containing increasing amounts of Et_3N (A) or DBU (B). (Quartz cuvette, pathlength 10 mm). The spectra of C_4F_9I, Et_3N and DBU in CH_3CN (1 ml) are reported for comparison.

Figure 4 shows the evolution of the absorbance of the C_4F_9I solutions at 365 and 405 nm as a function of the concentration of the Lewis bases. These graphs highlight the unusual behaviour of DBU. A linear increase of the absorbance at 365 nm is observed for TMG,

TMEDA, Et_3N and MTBD. This increase, ascribed to the increase in concentration of the C_4F_9I-Lewis base complexes, originates from the 290 nm absorption band tail. It should be noted that for the [C_4F_9I-MTBD] complex, which exhibits a very strong band at ~ 290 nm, the tail of this band leads to a significant and linear increase of the absorption at 405 nm when increasing the concentration of MTBD. For comparison, an absorbance of ~ 0.5 is observed at 405 nm for the C_4F_9I (0.46 M) / MTBD (0.45 M) mixture, compared to values < 0.05 for TMG, TMEDA and Et_3N. Interestingly with DBU, a marked increase of the absorbance is observed associated with a deviation from linearity when its concentration reaches ~ 0.3 M. As discussed above and in the ESI 2, this non-linear behaviour is directly related to the formation of the new species which generates a broad electronic absorption centered at ~ 420 nm.

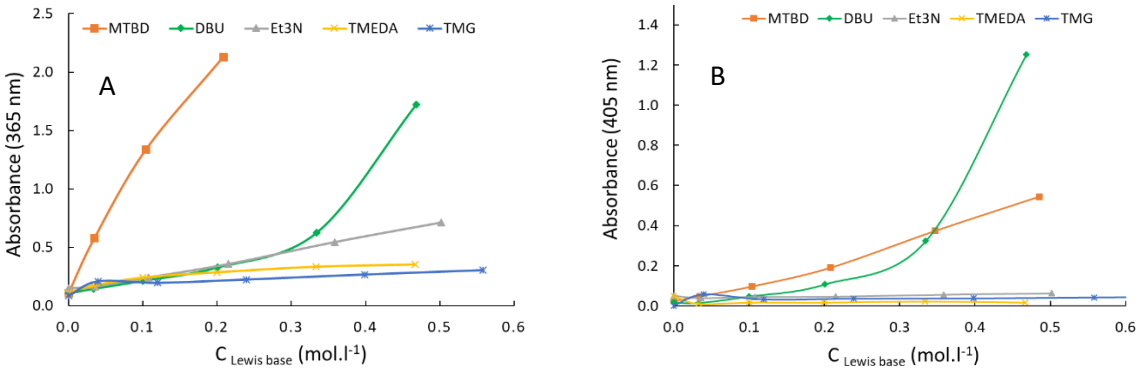

Figure 4: Evolution of the absorbance at 365 nm (A) and 405 nm (B) of CH_3CN solutions (1 ml) containing C_4F_9I (0.46 M) and a Lewis base in as a function of the Lewis base concentration (quartz cuvette, pathlength 10 mm).

3.2. Raman measurements

Raman measurements were carried out on the same mixtures as those studied by UV-Vis spectroscopy, where the C_4F_9I concentration is kept constant but the Lewis base concentration is varied. Although the Raman spectra have been measured in the spectral range 150 – 2000 cm^{-1}, figure 5 displays the spectra from 200 - 300 cm^{-1} where significant spectral variations were observed. Figure 5A shows the Raman spectra of CH_3CN solutions (1 ml) containing C_4F_9I (80 µl, 0.46 M) and increasing quantities of Et_3N (from 5 to 70 µl). Whereas Et_3N displays no contribution in the spectral range investigated, the spectrum of C_4F_9I exhibits a band at 279 cm^{-1} and two weak bands at 260 and 292 cm^{-1}. In agreement with previous reports [21, 22] and DFT calculations (see Figure S3 in ESI 3), the main band at 279 cm^{-1} is associated with the C−I stretching normal mode of C_4F_9I (coupled with a CF_2 wagging) that is free from any halogen bonding interaction. The two less intense bands are mainly associated to C−F deformation modes of the perfluoroalkyl chain. As the concentration of Et_3N increases, a significant decrease of the "free" C_4F_9I peak is observed while a new band at 263 cm^{-1} increases that can be assigned to the halogen bond complex between Et_3N and C_4F_9I (see DFT calculations below). For comparison, the Raman spectra of the C_4F_9I-DBU mixtures are reported in Figure 5B. Similarly to Et_3N, the spectrum of DBU in CH_3CN is silent in the range 200-300 cm^{-1}. Upon addition of increasing quantities of DBU to

the C_4F_9I-CH_3CN solution, the intensity of the "free" C_4F_9I peak strongly decreases, to almost vanish at the highest concentration of DBU investigated, suggesting that there is a low amount of "free" C_4F_9I left in solution in these conditions. Concomitantly, as observed with Et_3N, a new band assigned to a halogen bond complex between DBU and C_4F_9I emerges at about 263 cm^{-1} (see DFT calculations below). In addition, bands that were hardly detectable for "free" C_4F_9I at 225 and 240 cm^{-1} become apparent upon complex formation.

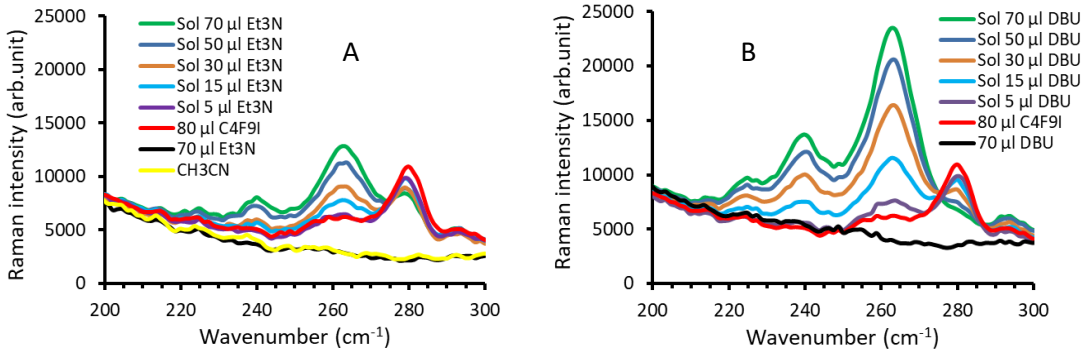

Figure 5: Raman spectra of solutions of C_4F_9I (80 µl, 0.46 M) in CH_3CN (1 ml) containing increasing amounts of Et_3N (A) or DBU (B) (Quartz cuvette, pathlength 10 mm). The spectra of C_4F_9I, Et_3N and DBU in CH_3CN (1 ml) are reported for comparison.

The comparison of the Raman spectra of CH_3CN solutions containing C_4F_9I (0.46 M) and Lewis bases (0.5 M) is reported in figure 6. Irrespective of the Lewis base, the intensity of the "free" C_4F_9I peak is strongly reduced while a new band at 263-266 cm^{-1} emerges, which is assigned to the halogen bond complex. Considering that the equilibrium constant could be estimated from the intensity ratio of the peaks of the "free" and complexed C_4F_9I,[29], it can be estimated that in the conditions of figure 6, for DBU, MTBD, TMG and TMEDA Lewis bases, that more than 80% of C_4F_9I molecules are engaged in an halogen bond complex, while about 50% of the C_4F_9I molecules remain uncomplexed with the Et_3N Lewis base.

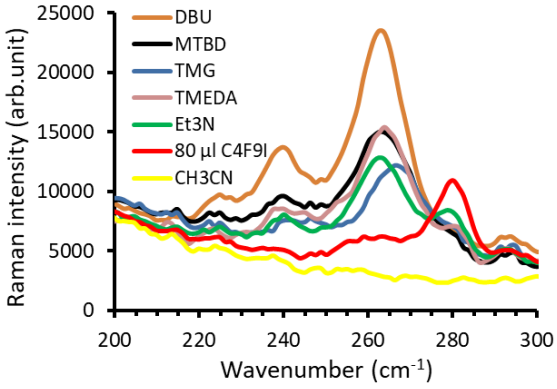

Figure 6: Raman spectra of solutions of C_4F_9I (80 µl, 0.46 M) in CH_3CN (1 ml) containing Lewis bases (0.5 M) (quartz cuvette, pathlength 10 mm). The spectrum of CH_3CN and C_4F_9I are reported for comparison.

3.3. DFT calculations on the [C_4F_9I-Lewis base] complexes

In order to correlate the observed evolution of the UV-Vis and Raman spectra with the halogen bond interactions, we performed DFT calculations on the [C_4F_9I-LB] complexes to evaluate their stabilization energies and calculate their Raman spectra. Among the DFT methods that have been tested, it was found that functionals with high exact exchange or long-range corrections were suitable for these complexes, especially M06-2X, ωB97XD, and double hybrids.[24] Thus, DFT calculations were performed using the M06-2X functional and the DGDZVP basis set.

3.3.1. Structural and energetic considerations

The fully optimized geometries of the isolated [C_4F_9I-DBU] and [C_4F_9I-Et_3N] complexes (Figure 7), were found to have intermolecular $R_{(I\cdots N)}$ distances of 2.80 and 2.86 Å, respectively (Table 1).

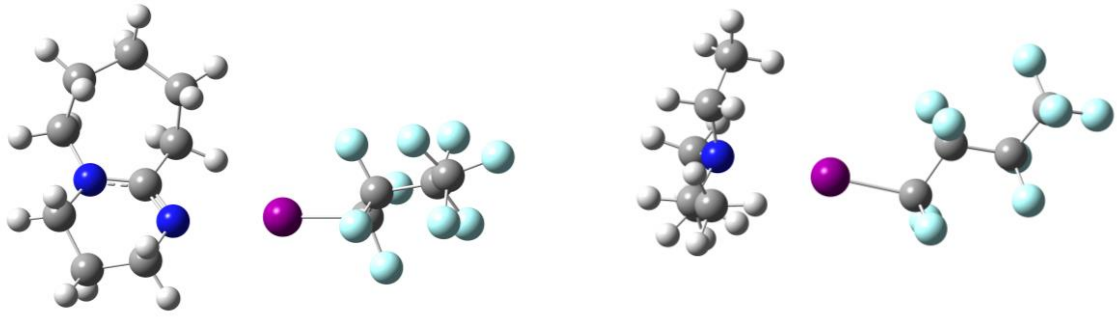

Figure 7: Optimized structures of the [C_4F_9I-DBU] and [C_4F_9I-Et_3N] complexes at the M06-2X level using the DGDZVP basis set.

In the complexes, the carbon-iodine axis points towards the nitrogen atom of DBU or Et_3N with an N-I-C angle close to 180° (177.4° and 178.2° with DBU and Et_3N, respectively), as expected for a HB interaction where the donating lone pair of the amine interacts with the σ-hole which develops on the iodine atom at the opposite of the CF_2–I bond axis. Such a configuration is found for all the Lewis bases investigated (see ESI 4) and is consistent with a halogen bonding interaction.[9] The distances between the iodine atom of C_4F_9I and nitrogen atoms of the Lewis bases are reported in table 1, as well as the calculated binding energies of the [C_4F_9I-LB] complexes. It appears that the calculated binding energies vary from 9.20 kcal mol^{-1} for the [C_4F_9I-TMG] complex, up to 10.82 kcal mol^{-1} for [C_4F_9I-DBU].
For comparison, calculations were carried out on a series of weaker nitrogen Lewis bases such as pyridine or aniline, but also oxygen in Lewis bases such as propylene oxide (PO), THF, acetone and dimethylacetamide (DMA), the latter two being used recently for the activation of perfluoroalkylation reactions.[10, 11] The energy minimized structures of the conformers for the [C_4F_9I-acetone] and [C_4F_9I-DMA] complexes are depicted in Figure 8.

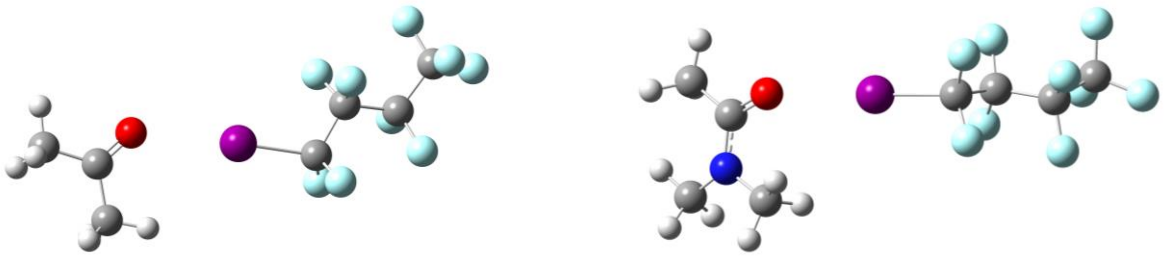

Figure 8: Optimized structure of the [C_4F_9I-acetone] and [C_4F_9I-DMA] complexes at the M06-2X level using the DGDZVP basis set.

Similarly to the nitrogen Lewis bases described above, the equilibrium geometries of the complexes are found with the iodine atom of C_4F_9I pointing towards an electron lone pair of the oxygen atom. The stabilization energies calculated at the M06-2X level are found to be lower, i.e. lying in the range of 6.01 kcal mol^{-1} for [C_4F_9I-PO] to 7.25 kcal mol^{-1} for [C_4F_9I-DMA].

Table 1: Interaction energies (ΔE), intermolecular $R_{(I\ldots N)}$ distances, calculated ($\nu_{(C\text{-}I)}$DFT) and experimental ($\nu_{(C\text{-}I)}$Exp) frequencies associated with the C−I stretching normal mode for the [C_4F_9I–LB] complexes calculated at the M06-2X level of theory using the DGDZVP basis set. The pKa (from ref. [30]) and pK_{BI2} (from ref. [31]) values of the Lewis bases are also reported.

Complex	$\Delta E_{M06\text{-}2X}$ (kcal mol^{-1})	$R_{(I\ldots N/O)}$ (Å)	$\nu_{(C-I)}$DFT[(a)] (cm^{-1})	$\nu_{(C\text{-}I)}$Exp (cm^{-1})	*pKa (CH$_3$CN)*	*pK_{BI2}*
C_4F_9I monomer	-	-	276.2	279	-	-
[C_4F_9I-DBU]	-10.82	2.797	265.4	263	24.3	-
[C_4F_9I-Et_3N]	-9.71	2.861	265.4	263	18.83	3.6
[C_4F_9I-TMG]	-9.20	2.892	269.5	266	23.35	4.37
[C_4F_9I-MTBD]	-10.06	2.831	266	263	25.47	-
[C_4F_9I-TMEDA]	-10.55	2.905	268.3	264	18.69	3.8
[C_4F_9I-Pyridine]	-7.08	2.924	270.9	270 [(b)]	12.53	2.22
[C_4F_9I-Aniline]	-6.47	3.008	271	274[(b)]	10.64	0.9
[C_4F_9I-THF]	-6.88	2.887	272.6	-	-	0.4
[C_4F_9I-Acetone]	-6.33	2.940	275.4	276[(b)]	-	0.05
[C_4F_9I-PO]	-6.01	2.899	274.3	-	-	-0.03
[C_4F_9I-DMA]	-7.25	2.863	274.5	-	-	1.18

(a) Scaled with a factor of 0.95 (from ref. [32])

(b) From ref. [22]

In order to rationalise such variations, we report in figure 9 the evolution of the calculated binding energies as a function of two different parameters which allow quantification of the Lewis basicity, namely pKa (in CH_3CN)[30] and pK_{BI2} (see table 1).[31] We remember that pK_{BI2} refers to the so-called diiodine basicity scale that is estimated from the equilibrium constant of the complex formation between iodine and a Lewis base.

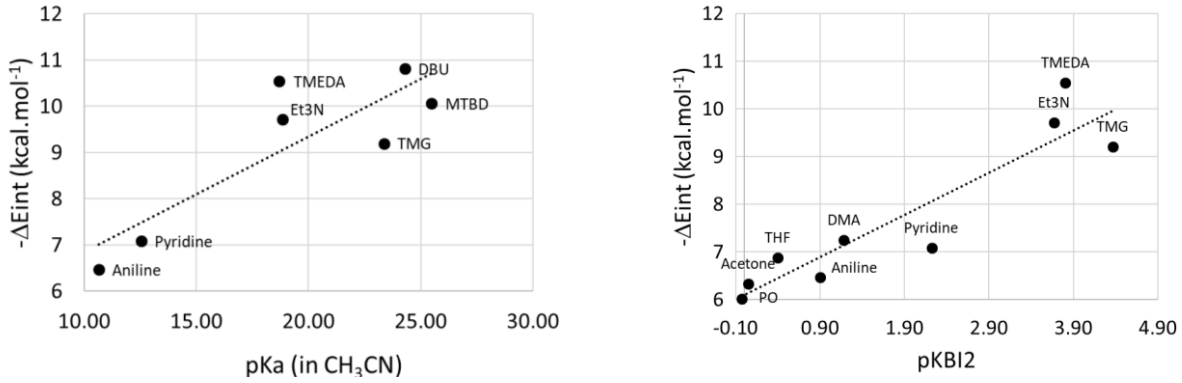

Figure 9: Plot of the calculated binding energies of the [C_4F_9I-LB] complexes as a function of the pKa (in CH_3CN) and the pK_{BI2} of the Lewis bases investigated in this study.

In particular, the pK_{BI2} scale is usually better adapted to evaluate the Lewis basicity of Lewis bases involved in halogen bond interactions. Thus, a general tendency is observed using both basicity scales: the higher the basicity of the Lewis base, the higher the strength of the binding energy between C_4F_9I and the Lewis base.

3.3.2. Vibrational spectra

In order to correlate the DFT calculations with the experimental Raman spectra, the vibrational analysis of the [C_4F_9I-LB] complexes has been performed starting from the optimized structures. In figure 10, the scaled calculated frequencies associated with the C−I stretching normal mode of C_4F_9I and its complexes are compared with the experimental values (Table 1). It appears that there is a good overall correlation between the theoretically predicted frequencies and those determined experimentally. Firstly, the absolute values calculated for both "free" C_4F_9I and the complexes are in a qualitative agreement. Secondly, the observed shift to lower frequencies for the C−I stretching normal mode in the complexes is well reproduced by the calculations. Indeed, all the computed frequencies in the complexes being lower than the one predicted for the "free" C_4F_9I.

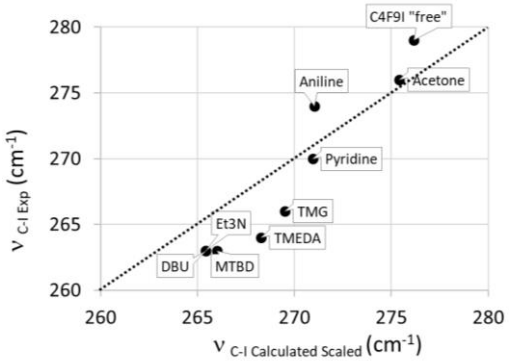

Figure 10: Comparison of the experimental and scaled calculated frequencies at the M06-2X/DGDZVP computational level of the C−I stretching normal mode of "free" C_4F_9I and [C_4F_9I-LB] complexes. A scaling factor of 0.95 was used to scale the calculated frequencies.[32]

As there is a good agreement between experimental and calculated frequency values of the C−I stretching normal mode, we can postulate that the calculated equilibrium geometry reported for the [C_4F_9I–LB] complexes should correspond to the most probable conformation in CH_3CN solution. By the same rationale, we observe in figure 11 that the calculated interaction energies between C_4F_9I and the Lewis bases are correlated to both the experimental and calculated frequencies of the C-I stretching normal mode of the [C_4F_9I-LB] complexes. Therefore, the strength of the halogen bond interaction that occurs between C_4F_9I and Lewis bases can be estimated through the amplitude of the frequency shift observed for the C-I stretching normal mode of C_4F_9I.

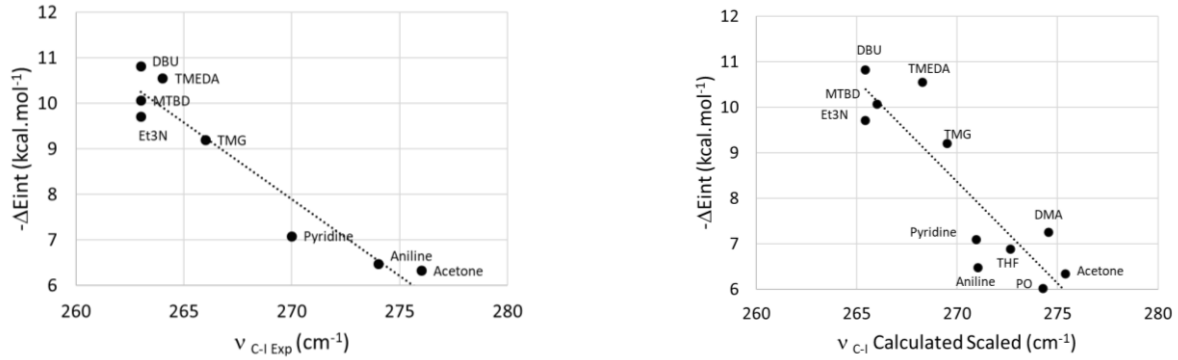

Figure 11: Evolution of the calculated binding energies as a function of the experimental and scaled calculated frequencies of the C−I stretching normal mode of [C_4F_9I-LB] complexes investigated in this study.

4. CONCLUSION

The halogen bonding interaction between a model Rf–I (C_4F_9I) and a series of Lewis bases that are used to initiate visible light promoted perfluoroalkylation reactions was investigated. The optical and vibrational properties of a range of [C_4F_9I-LB] complexes, including [C_4F_9I-DBU], [C_4F_9I-MTBD], [C_4F_9I-TMG], [C_4F_9I-TMEDA] and [C_4F_9I-Et_3N], have been characterized in acetonitrile solution, using UV-Visible absorption and Raman scattering combined with DFT calculations. In particular, the band at 279 cm^{-1} associated with the C−I stretching normal mode of C_4F_9I was shown to shift about 20 cm^{-1} towards lower wavenumbers upon formation of the halogen-bonded [C_4F_9I-LB] complexes. Additionally, the Raman study revealed that in the concentration conditions typically used for perfluoroalkylation reactions, the [C_4F_9I-LB] complexes are the main species present in CH_3CN. Interestingly, complex formation is characterized by a strong increase of the absorption from 225 - 350 nm, the absorption tail leading to low but significant absorption in the blue region of the optical spectra. We suspect that this residual absorption combined with blue light irradiation might promote the generation of small amounts perfluoroalkyl radicals that could initiate productive radical chain processes. Finally, the case of DBU warrants comment. A reaction between DBU and C_4F_9I occurs in the ground-state at room temperature,

which leads to the appearance of a yellow product. Whether this side-reaction, which is not observed with the other bases, will be beneficial or not in light-mediated perfluoroalkylations implying RfIs, is an open question, which maybe answered through additional future studies.

ACKNOWLEDGMENTS

The authors acknowledge the "Conseil Régional Nouvelle Aquitaine" (CRNA) for financial support for the purchase of infrared and Raman equipment. Computational time was provided by the Pôle Modélisation HPC facilities of the Institut des Sciences Moléculaires UMR 5255 CNRS − Université de Bordeaux and the "Mesocentre de Calcul Intensif en Aquitaine" (MCIA) co-funded by CRNA. The authors are also grateful to Dr. Nathan McClenaghan for careful and thorough reading of this manuscript.

REFERENCES

[1] M. Yan, J.C. Lo, J.T. Edwards, P.S. Baran, J. Am. Chem. Soc., 138 (2016) 12692-12714.
[2] N. Romero, D. Nicewicz, Chem. Rev., 116 (2016) 10075-10166.
[3] L. Marzo, S.K. Pagire, O. Reiser, B. König, Angew. Chem., Int. Ed., 57 (2018) 10034-10072.
[4] L. Buzzetti, G.E.M. Crisenza, P. Melchiorre, Angew. Chem., Int. Ed., 58 (2019) 3730-3747.
[5] C.G.S. Lima, T. de M. Lima, M. Duarte, I.D. Jurberg, M.W. Paixão, ACS Catal., 6 (2016) 1389-1407.
[6] G.E.M. Crisenza, D. Mazzarella, P. Melchiorre, J. Am. Chem. Soc., 142 (2020) 5461-5476.
[7] R.S. Mulliken, J. Am. Chem. Soc., 72 (1950) 600-608.
[8] A. Postigo, Eur. J. Org. Chem., 2018 (2018) 6391-6404.
[9] G. Cavallo, P. Metrangolo, R. Milani, T. Pilati, A. Priimagi, G. Resnati, G. Terraneo, Chem. Rev., 116 (2016) 2478-2601.
[10] T. Mao, M.J. Ma, L. Zhao, D.P. Xue, Y. Yu, J. Gu, C.Y. He, Chem. Commun., 56 (2020) 1815-1818.
[11] W.W. Xu, L. Wang, T. Mao, J. Gu, X.F. Li, C.Y. He, Molecules, 25 (2020) 508-516.
[12] Y. Wang, J. Wang, G.X. Li, G. He, G. Chen, Org Lett, 19 (2017) 1442-1445.
[13] Y. Liu, X.L. Chen, K. Sun, X.Y. Li, F.L. Zeng, X.C. Liu, L.B. Qu, Y.F. Zhao, B. Yu, Org. Lett., 21 (2019) 4019-4024.
[14] X. Sun, W. Wang, Y. Li, J. Ma, S. Yu, Org. Lett., 18 (2016) 4638-4641.
[15] D.E. Yerien, R. Conde, S. Barata-Vallejo, B. Camps, B. Lantaño, A. Postigo, RSC Adv., 7 (2017) 266-274.
[16] G.-R. Park, Y. Choi, M.G. Choi, S.-K. Chang, E.J. Cho, Asian Journal of Organic Chemistry, 6 (2017) 436-440.
[17] L. Helmecke, M. Spittler, K. Baumgarten, C. Czekelius, Org Lett, 21 (2019) 7823-7827.
[18] W. Lecroq, P. Bazille, F. Morlet-Savary, M. Breugst, J. Lalevee, A.C. Gaumont, S. Lakhdar, Org Lett, 20 (2018) 4164-4167.
[19] L. Wozniak, J.J. Murphy, P. Melchiorre, J. Am. Chem. Soc., 137 (2015) 5678-5681.
[20] R. Beniazza, L. Remisse, D. Jardel, D. Lastecoueres, J.M. Vincent, Chem. Commun., 54 (2018) 7451-7454.
[21] M.T. Messina, P. Metrangolo, W. Navarrini, S. Radice, G. Resnati, G. Zerbi, J. Mol. Struct., 524 (2000) 87-94.
[22] L.K. Mork, V. Tat, D.J. Ulness, B.G. Erickson, M.W. Gealy, J. Mol. Liq., 271 (2018) 647-654.
[23] M.G. Sarwar, B. Dragisic, L.J. Salsberg, C. Gouliaras, M.S. Taylor, J. Am. Chem. Soc., 132 (2010) 1646-1653.

[24] S. Kozuch, J.M. Martin, J Chem Theory Comput, 9 (2013) 1918-1931.
[25] E. Tannenbaum, E.M. Coffin, A.J. Harrison, J. Chem. Phys., 21 (1953) 311-318.
[26] I. Kaljurand, T. Rodima, I. Leito, I.A. Koppel, R. Schwesinger, J. Org. Chem., 65 (2000) 6202-6208.
[27] M. Carafa, E. Mesto, E. Quaranta, Eur. J. Org. Chem., 2011 (2011) 2458-2465.
[28] L.L. McCoy, D. Mal, J. Org. Chem., 46 (1981) 1016-1018.
[29] C.D. Schmulbach, R.S. Drago, J. Am. Chem. Soc., 82 (1960) 4484-4487.
[30] S. Tshepelevitsh, A. Kütt, M. Lõkov, I. Kaljurand, J. Saame, A. Heering, P.G. Plieger, R. Vianello, I. Leito, Eur. J. Org. Chem., 2019 (2019) 6735-6748.
[31] C. Laurence, J.-F. Gal, Lewis Basicity and Affinity Scales: Data and Measurement., John Wiley & Sons Ltd: Chichester, U.K. 2010.
[32] M.K. Kesharwani, B. Brauer, J.M. Martin, J. Phys. Chem. A, 119 (2015) 1701-1714.